

Properties of Microwaves

PY4113 Lab Report

University College Cork
School of Physics

Author: Jordan Darran Emmett Walsh (120387836)

Lab Partner: Rory Fox

Location: Kane Building G06, University College Cork

Date: 05/10/23, 06/10/23

Contents

Introduction	2
1.1 Motivation	2
1.2 Fundamentals	2
Experiments	4
2.1 Polarisation	5
2.1.1 Direct Polarisation	5
2.1.2 Cross Polarisation	6
2.2 Reflection, Standing Waves, and the Speed of Light	6
2.2.1 Law of Reflection	6
2.2.2 Direct Standing Waves and Wavelength Measurement	7
2.2.3 Oblique Standing Waves	9
2.3 Antenna and Aperture Radiation Patterns	10
2.3.1 Single Slit Diffraction	10
2.3.2 Double Slit Diffraction	11
2.4 Refraction	12
2.5 The Influence of Humidity on Microwave Propagation	13
2.6 Reflection by the Ionosphere (Lloyd's Mirror)	14
2.7 Microwave Interferometry	16
2.7.1 Michelson-Morley Interferometer	16
2.7.2 Fabry-Perot Interferometer	17
2.7.3 Thin Film Reflections	19
Further Discussion	20
Conclusion	21

Properties of Microwaves

Introduction

This report details one of five experiments completed as part of enrollment in PY4113. The objective of this experiment is to demonstrate various wave properties of microwaves.

The report is structured atypically. Since there are multiple experiments and demonstrations, each topic is covered in the style of independent sub-reports containing the typical sections on setup, procedure, results and all contain discussion independent of each other. The report finishes with a more general discussion regarding sources of experimental error and attempts to cross reference results/conclusions from sub-reports.

1.1 Motivation

Microwaves are electromagnetic waves that operate within the frequency range 300 MHz up to 300 GHz [1].

The most notable application of microwaves is the *microwave oven* [1]. They work by emitting microwave radiation which cause water molecules in food to vibrate through a process called dielectric heating. Dielectric heating is the stimulation of dipolar molecules (water molecules) in a dielectric medium at high speed, resulting in a conversion of electromagnetic to kinetic energy and causing friction between molecules [2]. Microwave radiation has been used to induce this effect as a medical procedure to treat atrial fibrillation [2].

Microwave dielectric heating has also become an established technique in synthetic organic chemistry, where the discussed phenomenon proves useful by reducing reaction times for chemical synthesis [3].

Microwaves are utilised and investigated extensively in Radio Astronomy [4]. The Cosmic Microwave Background (CMB) is a remnant of the very beginning of the universe, light which has cooled and weakened considerably and now classed as microwaves. CMB has been considered one of the most powerful tools in Cosmology and continues to provide insights of the early universe [5].

1.2 Fundamentals

Electromagnetic wave properties include polarisation, reflection, diffraction, and refraction, all of which are demonstrated throughout. This section gives a brief outline of relevant theory and makes note of specific details which will be later referenced.

Polarisation

Polarisation is a property of light waves where oscillations of electric and magnetic fields occur in a specific direction. When light is polarized, its waves vibrate predominantly in one plane, filtering out vibrations in other directions.

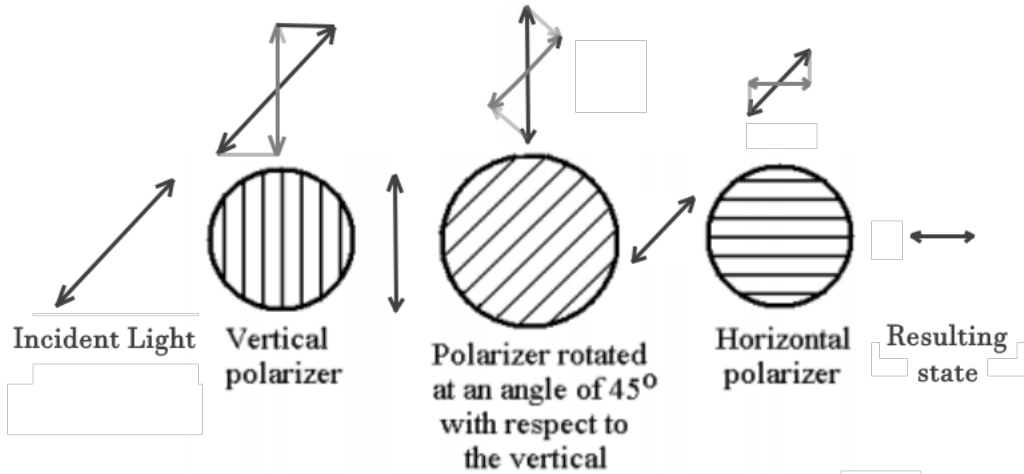


Figure 1.1: Graphical demonstration of polarisation by means of filtering. Vector diagrams shown above filters show how the incident wave is broken down into subsequent components as it propagates through the polarising filters.

A polarised filter breaks the wave down into subsequent components, as demonstrated in Fig 1.1. Note that in Fig 1.1 the resulting state of the 45° filter appears half in magnitude of the first polarised state (Vertical polariser).

Reflection

Reflection is the phenomenon in which waves, such as light or sound, encounter a surface or boundary and change direction.

The law of reflection states that the angle at which a wave is incident on a boundary is equal to the angle at which it is reflected. Mathematically (with reference to Fig 1.2) this reads

$$\phi_i = \phi_r = \frac{\Delta\phi}{2} \quad (1.1)$$

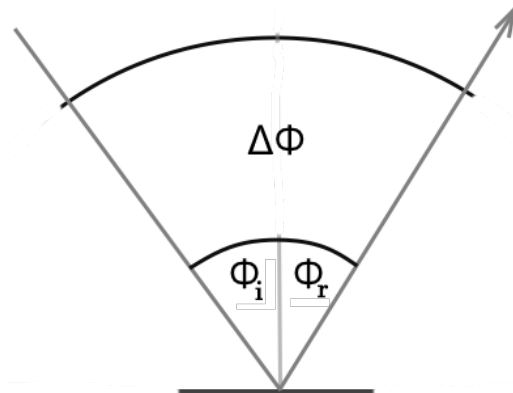
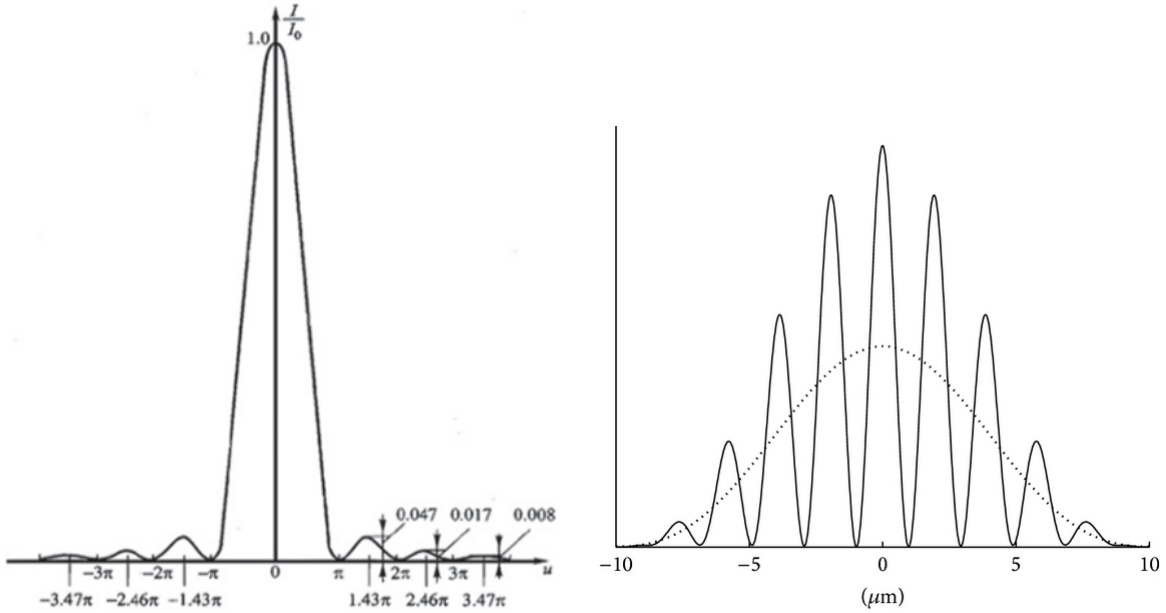


Figure 1.2: Supplementary figure for the law of reflection.

Diffraction

Diffraction is the process through which waves, such as light or sound, bend and spread as they encounter an obstacle or aperture. The Huygens–Fresnel principle states that every point on a wavefront is itself a source of spherical wavelets, which all mutually interfere [6]. Fig 1.3 shows the resulting intensity patterns for double and single slit apertures under this treatment.



(a) Single Slit Fraunhofer Diffraction Pattern [7].

The function is described by $\text{sinc}^2(u) = \frac{\sin^2(u)}{u^2}$

(b) Double Slit Diffraction Pattern for a

simulated optical setup [8].

Figure 1.3: Relevant diffraction patterns for this report. In the double slit setup (b), for light detected at an angle θ , constructive interference occurs when $m\lambda = d\sin(\theta)$ where m a positive integer and d is the distance between the slits. In (a), note that minima are not centered between points of maxima.

Refraction

Refraction is an effect where waves change direction as they pass from one medium to another with differing refractive indices. This can be described by Snell's law which states

$$n_1 \sin(\theta_1) = n_2 \sin(\theta_2) \quad (1.2)$$

where n_x is refractive index of medium x and θ_x is the angle of propagation from the boundary normal in medium x . Snell's law can be utilised to solve for deflection angles of various setups.

Experiments

This section details experiments carried out to demonstrate the discussed wave-properties.

Apparatus: Microwaves were transmitted and detected using the Central Scientific Company 3cm Microwave Apparatus (*Catalog No 36811*). This kit is comprised of a microwave transmitter and receiver (each with directive gain horns), a turn table mount with rotatable arms, and a number of cards with metallic elements/patterns that work effectively as reflectors, polarisers, and apertures. There are 2 aperture cards with single and double slits for demonstrating related diffraction patterns. See [9] for a full list of parts and accessories.

2.1 Polarisation

The transmitter of the Microwave Apparatus emits microwaves in the $\text{TE}_{1,0}$ mode [9]. Therefore, the \mathbf{E} field is transverse to the direction of propagation. This field is generated using a Gunn Diode, (see [9] for specific details). "The Gunn diode in its mount produces vertical linear polarized monochromatic energy, (at a single frequency), which is radiated by the flared horn." [9] The receiver contains a point contact silicon junction and is supported in a waveguide mount, "The assembly can be positioned for either vertical or horizontal electric field polarization." [9] Therefore we consider two cases; Direct and Cross polarisation.

2.1.1 Direct Polarisation

Setup/Procedure

The experiment was setup as shown in Fig 2.4 with the transmitter turned on and receiver gain adjusted to a centre reading ($25\mu\text{A}$) when no polariser was present. A polarised grating was introduced about 2.5cm from the receiver horn and it's effect was investigated for various orientations.

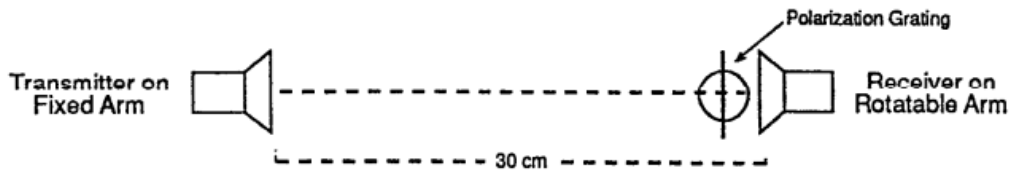


Figure 2.4: [9] Experimental setup for direct and cross polarisation. The transmitter and receiver were spaced 30cm apart. The polarised grating was held about one inch in front of and parallel to the receiver horn aperture. When rotating the polariser a protractor was used to accurately determine the angle of polarisation.

Results/Discussion

Tab 2.1 shows the effect of introducing and rotating the polarised grating. The polarisation dependence of the receiver is evident. As we expect from the discussion in 1.2, at 45° the power is effectively halved, while at 90° microwaves are no longer detected. When the polarised grating is in-line with the transmitter polarisation (0°) there is effectively no change.

Polarisation Angle ($^\circ$)	Intensity (μA)
0	21 ± 0.5
90	2 ± 0.5
45	12 ± 3.0

Table 2.1: Direct Polarisation experimental data. Before introducing the polariser the receiver read $25\mu\text{A}$. Polarisation Angle represents the angle of the grating strips to the horizontal i.e. 90° corresponds to grating strips oriented perpendicular to the worktop. Uncertainties are based off of receiver intensity fluctuations and are due to human error; the polariser was held and oriented by hand.

2.1.2 Cross Polarisation

Setup/Procedure

The experiment was setup as shown in Fig 2.4 with the transmitter rotated 90° to it's orientation in 2.1.1. Without a polariser, there was no detected intensity analogous to previous discussion. The gain was not altered from it's setting in 2.1.1 and the followed procedure was identical to that outlined in 2.1.1.

Results

Tab 2.2 shows the effect of introducing and rotating the polarised grating. Analogous to the discussion in 1.2 (See Fig 1.1) we expect maximum detected intensities at polarisations 45° to the initial transmitted wave. This effect is evident and we see identical results at 45° when compared to Tab 2.1.

Polarisation Angle (°)	Intensity (μA)
0	1 ± 0.5
27.5	5 ± 4.0
45	12 ± 3.0
67.5	5 ± 5.0
90	0.5 ± 5.0
-45	12 ± 3.0

Table 2.2: Cross Polarisation experimental data. Before introducing the polariser the receiver read $\approx 0\mu\text{A}$. Polarisation Angle represents the angle of the grating strips to the horizontal i.e. 90° would correspond to grating strips oriented perpendicular to the worktop. 45° and -45° represent orthogonal polarisation states. Uncertainties are based off of receiver intensity fluctuations and are due to human error; the polariser was held and oriented by hand.

2.2 Reflection, Standing Waves, and the Speed of Light

2.2.1 Law of Reflection

Setup/Procedure

The experiment was setup as shown in Fig 2.5. The reflecting card/grid was placed in the centre of the turntable and the transmitter was turned on. For a given grid orientation, θ_{grid} , the receiver was rotated about the central pivot in a region where we would typically expect reflection. The angular locations of maximum detected intensity, $\max \phi_{receiver}$, were documented for each case.

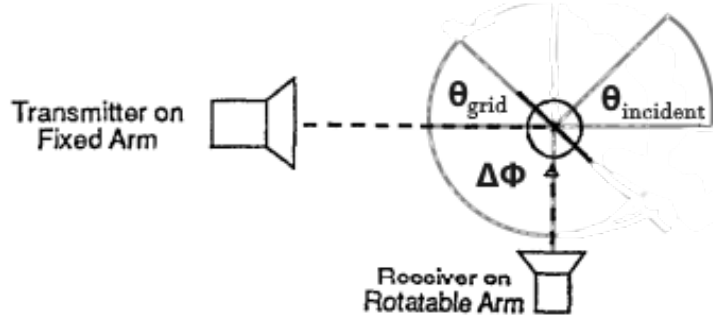


Figure 2.5: [9] with additional annotation. Experimental setup for demonstrating law of reflection. $\Delta\phi$ and θ_{grid} are the angle between emitter and receiver when reading maximum intensity. θ_{grid} represents the grid orientation to the transmitter. $\theta_{incident}$ represents the resulting incident angle of microwaves. See Tab 2.3 for resulting data.

Results/Discussion

θ_{grid} (°)	$\theta_{incident}$ (°)	$\phi_{emitter}$ (°)	max $\phi_{receiver}$ (°)	$\Delta\phi$ (°)
45	45	178	87	91
32	58	178	64	114
62	28	178	120	58
75	15	178	141	37

Table 2.3: Experimental data analogous to setup in Fig 2.5. θ_{grid} represents the grid orientation to the transmitter. $\theta_{incident}$ represents the resulting incident angle of microwaves. $\phi_{emitter}$ is the position of the microwave emitter as read from the protractor on the turn table and remained fixed. max $\phi_{receiver}$ is the position of the microwave receiver with a maximum intensity reading as read from the protractor on the turn table. $\Delta\phi = \phi_{emitter} - \max \phi_{receiver}$ and is the angle between emitter and receiver when reading maximum intensity.

The resulting data of the outlined procedure is shown in Tab 2.3. It is evident from the results that for all demonstrated cases of θ_{grid}

$$\frac{\Delta\phi}{2} \approx \theta_{incident}$$

This was the expected result analogous to the discussion in 1.2 and verifies the law of reflection (Eq. 1.1). Since this is a demonstration and there is no analytical calculation, an error analysis would not provide additional insight.

2.2.2 Direct Standing Waves and Wavelength Measurement

Standing waves are specific cases of superposition of two waves with the same frequency and amplitude traveling in opposite directions which create nodes of null intensity at **half-wavelength** intervals.

Setup/Procedure

The experiment was setup as shown in Fig 2.6. The procedure was followed as specified in [9] with one modification. That is, the position of the reflecting grid was

carefully altered from an initial position where the detected intensity was minimum, $d_{min,0}$. The distance between the initial position, $d_{min,0}$, and the 3rd consecutive position of detected minimum, $d_{min,3}$, were recorded (denoted Δd in Tab 2.4) For various initial conditions of $d_{min,0}$ an implied microwave half-wavelength can be calculated as $\frac{\lambda}{2} = \frac{\Delta d}{3}$.

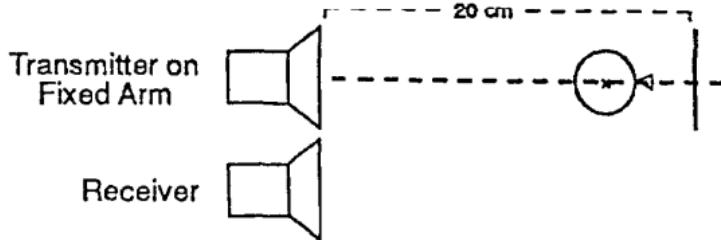


Figure 2.6: [9] Experimental setup for demonstrating standing waves and measuring the wavelength of emitted microwaves. The receiver was placed beside the transmitter and detected microwaves reflected off of the grid. The detected intensity of microwave radiation was dependant on the perpendicular distance of the grid from the transmitter/receiver horns. The difference in grid position between 2 consecutive detected minimas is half the wavelength of the transmitted radiation.

Results

$d_{min,0}$ (cm)	$d_{min,3}$ (cm)	Δd (cm)	$\frac{\lambda}{2}$ (cm)	λ (cm)
43.3	38.8	4.5	1.5	3.0
38.8	34.2	4.6	1.53333	3.06667
34.2	30.0	4.2	1.4	2.8
30.0	25.6	4.4	1.46667	2.93333

$$\bar{\lambda} = 2.95\text{cm} \mid \sigma_\lambda = 0.0986\text{cm}$$

Table 2.4: Experimental data analogous to setup in Fig 2.6. The distance between multiple sets of 3 consecutive minimas were recorded to use in calculation in an effort to reduce the potential for systematic error. $d_{min,0}$ represents the position of the grid at a starting minimum and $d_{min,3}$ represents the position of the grid after moving 3 consecutive minimas. Δd is the distance between these points. $\frac{\lambda}{2} = \frac{\Delta d}{3}$ from which an implied microwave wavelength can be determined. $\bar{\lambda}$ is the mean wavelength determined. σ_λ is the standard deviation of determined wavelengths.

From the data and analysis in Tab 2.4, we can conclude the wavelength of the microwaves to be

$$\lambda = (2.95 \pm 0.0986)\text{cm} \quad (2.3)$$

This is just within the margin of error of the wavelength cited in [9] (2.85cm). [9] states the transmitter frequency to be $f = 10525\text{MHz}$, implying a speed of light

$$\begin{aligned} c &= f\lambda \\ &= (10.525 \times 10^9\text{Hz})(0.0295\text{m}) \\ &= 31048750000\text{ms}^{-1} \\ &= 3.105 \times 10^8\text{ms}^{-1} \end{aligned}$$

Error Analysis

An appropriate error for c can be determined from σ_λ by utilising

$$\begin{aligned}\frac{\Delta c}{c} &= \frac{\Delta \lambda}{\lambda} = \frac{\sigma_\lambda}{\lambda} \\ \implies \Delta c &= c \frac{\Delta \lambda}{\lambda} \\ &= (31048750000ms^{-1}) \left(\frac{0.0986cm}{2.95cm} \right) \\ &= 0.104 \times 10^8 ms^{-1}\end{aligned}$$

Allowing us to conclude

$$c = (3.105 \pm 0.104) \times 10^8 ms^{-1} \quad (2.4)$$

According to 'The International System of Units (SI)' brochure the actual speed of light is $299,792,458ms^{-1}$ [10], which lies within our determined margin of error. The relative error of our answer is

$$\begin{aligned}\epsilon_c &= \frac{(3.105 - 2.998) \times 10^8 ms^{-1}}{(2.998) \times 10^8 ms^{-1}} \\ &= +3.5\%\end{aligned}$$

2.2.3 Oblique Standing Waves

Setup/Procedure

The experiment was setup as shown in Fig 2.10. The procedure was followed as specified in [9]. Phase wavelengths for multiple positions of the reflecting grid from the pivot were determined. By moving the receiver, the distances between initial positions of detected minima and the 3rd consecutive positions of detected minima, $D_{min,3}$, were recorded. The corresponding phase wavelength for each case was then $\lambda_{ob} = 2 \times \frac{D_{min,3}}{3}$.

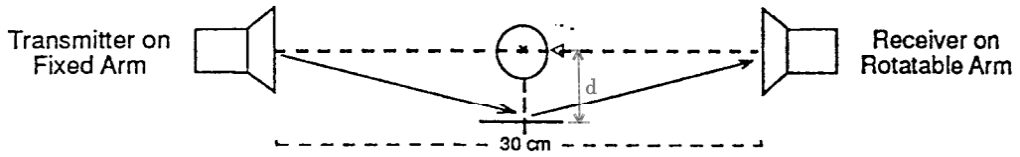


Figure 2.7: [9] Experimental setup used to determine phase wavelengths for various locations of a reflecting grid facing perpendicular to the direction of microwave propagation at a fixed distance d from the turn-table pivot.

Results/Discussion

The resulting data of the described procedure is shown in Tab 2.5. The results are not particularly interesting other than showcasing the existence of oblique standing waves and demonstrating that phase wavelength is dependant on the position of a reflecting surface. As discussed in [9] the phase wavelengths are longer than free-space wave lengths because the two interfering waves are travelling at oblique angles.

d (cm)	$D_{min,3}$ (cm)	λ_{ob} (cm)
6 ± 0.1	4.8 ± 0.1	3.2 ± 0.066
8 ± 0.1	5 ± 0.1	3.333 ± 0.066
10 ± 0.1	5 ± 0.1	3.333 ± 0.066
14.5 ± 0.1	6 ± 0.1	4 ± 0.066
21 ± 0.1	4.5 ± 0.1	3 ± 0.066

Table 2.5: Experimental data for oblique standing waves and determination of phase wavelength. d represents the fixed distance of the reflective grating from the turn-table pivot. $D_{min,3}$ represents the distances between initial positions of detected minima and the 3rd consecutive positions of detected minima. λ_{ob} is the resulting phase wavelength, which changed depending on the distance d .

2.3 Antenna and Aperture Radiation Patterns

This section demonstrates techniques for measuring directivity patterns of radiating apertures and the directivity of the flared horns. The larger an antenna's aperture is in terms of wavelength; the more directive it's intensity pattern is, and the greater its gain and signal pick-up will be [9].

2.3.1 Single Slit Diffraction

Setup/Procedure

The experiment was setup as shown in Fig 2.8, with the transmitter horn moved close to the central axis of the turntable and the single slit accessory card placed approximately 2cm from the transmitter horn at the centre of the turn table. The procedure outlined in [9] did not produce satisfactory results for reasons which will be discussed later. Rather than locating an arbitrary maximum intensity about the central axis of the transmitter horn and then rotating the receiver about the central pivot to plot the interference pattern; a reliable radius of rotation was instead found by trial and error.

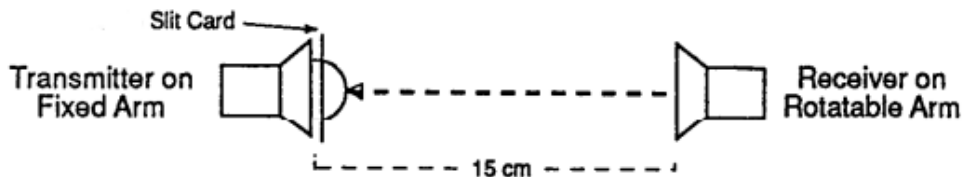


Figure 2.8: [9] Experimental setup for double and single slit diffraction demonstrations. The card was placed approximately 2.5cm from the emitter horn. The

A procedure to do so that is somewhat repeatable starts by rotating the receiver arm approximately 60° from the central position shown in Fig 2.8. Then with the receiver at an arbitrary distance from the fixed point of rotation, rotate the arm slowly back towards the centre and observe the detected intensity fluctuations. Repeat this for various radii of rotation until a location with strong and evident intensity fluctuations is found. Then at this improved radius, follow the steps outlined in [9], plotting the meter reading vs. angle off axis every 5° .

Results/Discussion

Fig 2.10 plots the resulting data of the outlined procedure. The resulting diffraction pattern appears similar to a $\text{sinc}(\phi)$ function. This is expected as per discussion in 1.2. This is most evident by the shape of the right hand side (positive off-angles), where minima are **not** centralised between maxima; a feature of the sinc function as mentioned previously.

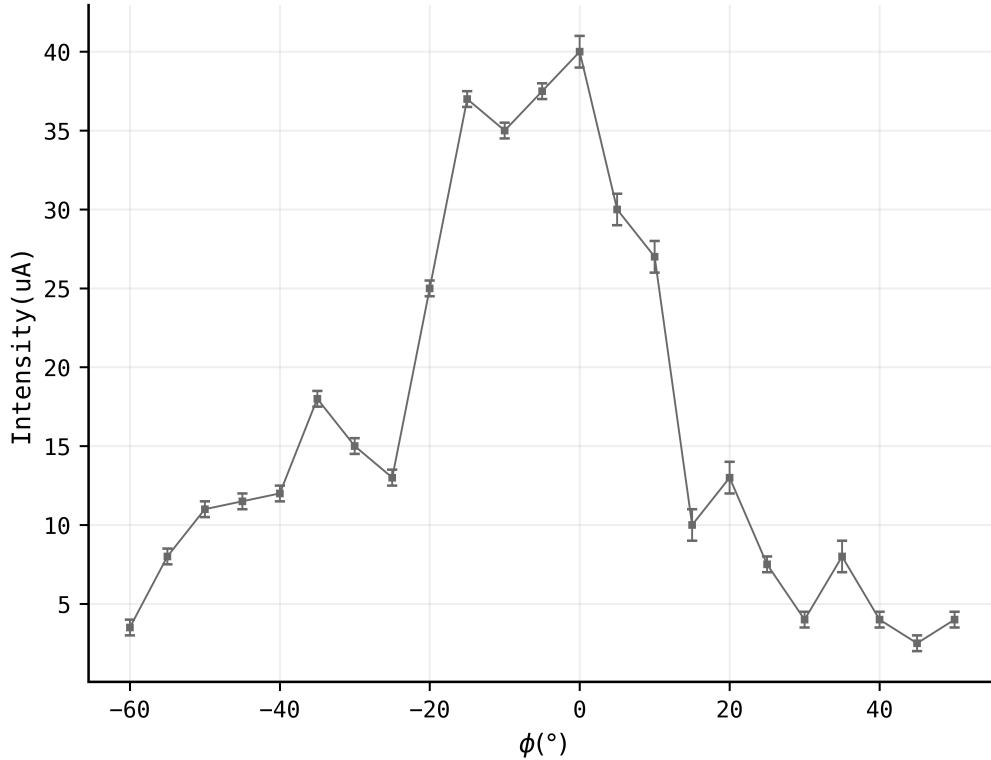


Figure 2.9: Plotted experimental data analogous to setup in Fig 2.8. ϕ represents the angular position of the receiver on the turntable when reading. The uncertainties in Intensity represent the observed intensity fluctuation at that point. The observed pattern is similar to a $\text{sinc}(\phi)$ function, which is what would be expected for single slit diffraction analogous to discussion in 1.2.

2.3.2 Double Slit Diffraction

Setup/Procedure

The experiment was setup as shown in Fig 2.8 and 2.10, with the double slit card in place of the single. Unlike the single-slit procedure, the procedure outlined in [9] produced satisfactory results and was followed verbatim.

Results/Discussion

The resulting data shows an interference pattern as expected from the discussion in 1.2. We observe minimum peaks at $\pm 20^\circ$ and $\pm 60^\circ$ as mentioned to be expected in [9].

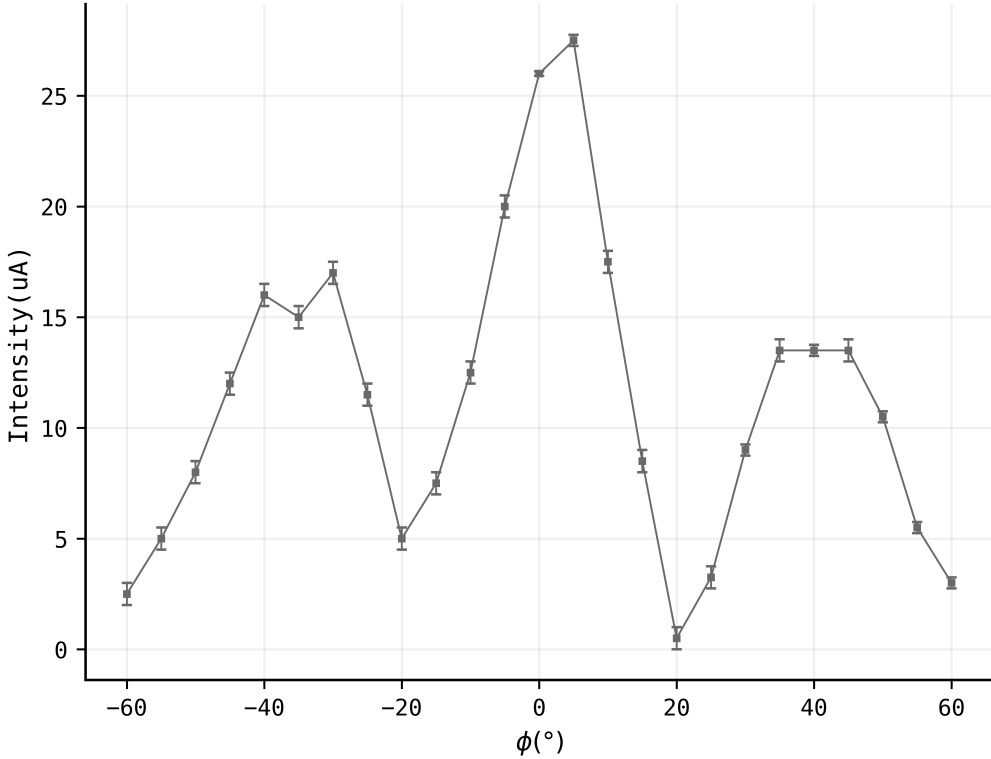


Figure 2.10: Plotted experimental data analogous to setup in Fig 2.8. ϕ represents the angular position of the receiver on the turntable when reading.

2.4 Refraction

Setup/Procedure

The experiment was setup as shown in Fig 2.11, with a styrofoam prism placed in the center of the turn table with it's apex pointed to the 270° mark. The prism was filled with various "dry-fill"^[9] dielectric materials (Wax, Glass Beads) and the resulting angle of deflection due to refraction was determined by rotating the receiver arm about the pivot and reading the angle at which maximum intensity was observed, $\max \phi_{receiver}$. Then by rotating the prism half of the observed $\max \phi_{receiver}$ such that the apex moved toward the receiver, the resulting deflections were determined and close to identical. From this a more accurate measure of the prism deflection angle, $\Delta\phi_{material}$, could then be determined. [9] states that Snell's law can be used to show the refractive index of the material corresponds to

$$0.30n = \sin \left(\frac{\Delta\phi}{2} + 17.5^\circ \right) \quad (2.5)$$

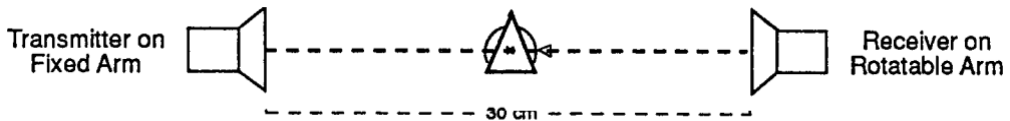


Figure 2.11: [9] Experimental setup for refraction demonstration.

Results/Discussion

Prism Pointer (°)	$\max \phi_{receiver}$ (°)	Material	$\Delta\phi$ (°)
270 ± 0.25	1 ± 1	No Material	
270 ± 0.25	19 ± 1	Glass Beads	19 ± 1.25
270 ± 0.25	10 ± 1	Wax	10 ± 1.25
279.5 ± 0.25	31 ± 1	Glass Beads	21.5 ± 1.25
275 ± 0.25	12.5 ± 1	Wax	7.5 ± 1.25

$$\Delta\phi_{Glass} = 20.25 \pm 1.25 \quad \Delta\phi_{Wax} = 8.75 \pm 1.25$$

Table 2.6: Experimental Data from procedure discussed above. $\Delta\phi_{Glass}/\Delta\phi_{Wax}$ is the determined prism deflection angle for glass beads/wax and the uncertainty was determined by taking the standard deviation of the raw data for respective $\Delta\phi$'s in the table. It is a coincidence that these match the experimental uncertainty. 'Wax' refers to paraffin wax.

Tab 2.6 shows the resulting data of the outlined procedure. The resulting refractive indices from determined $\Delta\phi$'s according to Eq. 2.5 are shown in Tab 2.7.

n_{Glass}	1.545 ± 0.095
n_{Wax}	1.241 ± 0.177

Table 2.7: Calculated microwave refractive indices according to Eq. 2.5. Uncertainties based off of uncertainty in $\Delta\phi$, where $\frac{\Delta n}{n} = \frac{\Delta\phi}{\phi}$. 'Wax' refers to paraffin wax.

It is difficult to compare our value for n_{Glass} , as this specific case is difficult to source in literature. One might argue that our answer for n_{Glass} aligns within the margin of error of crown glass (BK7) $n_{BK7} = 1.5168$ [11]. However, it is common knowledge and shown many times that refractive index can vary with the frequency/wavelength of radiation [11][12][13]; materials may have distinct responses to the frequency of electromagnetic waves. We see this, for example, in the dispersion of visible light from a prism. So our answer shouldn't necessarily be directly compared to the common source refractive indices of glasses. [14] states "*Paraffin is a variable mixture of alkanes (C_nH_{2n+2}), characterized by refractive indices ranging from 1 to 1.4, in case of microwaves*" which aligns well with our answer of $n_{Wax} = 1.241$.

2.5 The Influence of Humidity on Microwave Propagation

Setup/Procedure

The procedure and setup was followed verbatim to [9], where transmitter and receiver horns faced each other directly and spaced approximately 30cm apart, similar to the setup in 2.1.1. Under various conditions, a cloth was hung at the mid-point between transmitter and receiver horns to analyse induced effects. These conditions are noted in Tab 2.8.

Results/Discussion

Interference Material	Intensity (μA)	Notes
N/A (free space)	25 ± 0.5	
Dry Cloth	25 ± 0.5	Not Folded
	24.5 ± 0.5	Folded x1
	24 ± 0.5	Folded x2
	23.5 ± 0.5	Folded x3
Wet Cloth	11 ± 1	Not Folded
	6 ± 0.5	Folded x1
	1 ± 0.5	Folded x2

Table 2.8: Experimental Data demonstrating the effect of humidity on microwave propagation. Uncertainty in measurements correlates to intensity fluctuation present when measuring. There is a stark contrast between the wet cloth measurements and the dry cloth. Humidity has a major impact on microwave propagation.

It is very clear from Tab 2.8 that humidity has a major effect on microwave propagation. This is expected according to literature, [15] states "*large bandwidth microwave signals propagating in dispersive media can result in pulses decaying according to a non-exponential law.*"^[15]. Our setup is too crude to demonstrate such a relationship rigorously. For the wet cloth, Tab 2.8 shows that folding the cloth once made the intensity drop by approximately $\frac{1}{2}$. [15] found that while this was the case for fresh water, it was not for salt water as ionic currents gave a "*huge imaginary permittivity*"^[15] which overcame the permittivity of pure water. We did not have the materials present to demonstrate this.

2.6 Reflection by the Ionosphere (Lloyd's Mirror)

Humphrey Lloyd was an active Irish physicist in the 1800s. In Lloyd's experiment a beam splitter is used to create two light paths: one light beam reflects off a mirror, while the other beam reflects off a glass plate. When the reflected beams are recombined, they create an interference pattern [16]. The setup demonstrated is analogous to 'radio-fading', which occurs when there are significant variations in received signal amplitude and phase over time or space - this was a problem in car radio systems before automatic volume control was developed.

Consider the setup in Fig 2.12. It can be shown geometrically that

$$h_n = \sqrt{\left(\frac{nd\lambda}{2}\right) + \left(\frac{n^2\lambda^2}{4}\right)} \quad (2.6)$$

where h_n are the mirror heights at which we expect minimum signal, d is the distance between relevant transmission/receiving points and n is a positive integer.

Setup/Procedure

The experiment was setup as shown in Fig 2.12, with d , the distance between transmitter/receiver horns, set exactly to 61cm. The ionosphere was simulated using a metal sheet fixed in place using a laboratory stand with its face parallel to the tabletop as shown. The ionosphere's height above the receiver horn was slowly increased and each height of minimum detected intensity, h , was recorded. These heights are compared to the predicted according to Eq. 2.7.

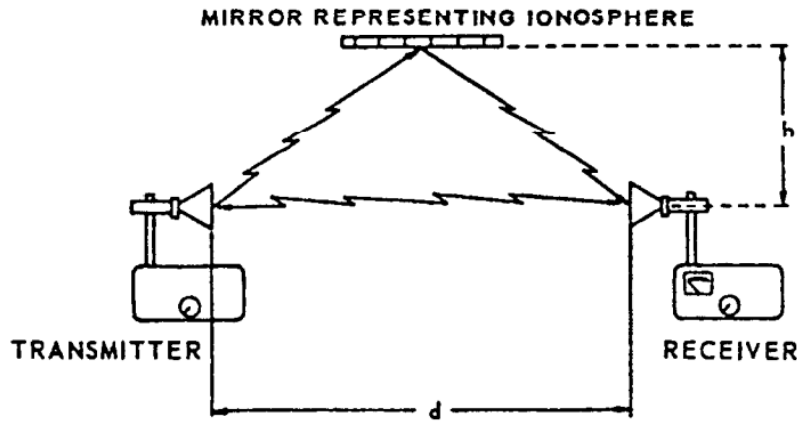


Figure 2.12: [9] Experimental setup used to demonstrate 'radio fading'. The ionosphere was simulated using a metal sheet fixed in place using a laboratory stand with its face parallel to the tabletop. Here $d = 61\text{cm}$.

Results/Discussion

The resulting data of the outlined procedure is shown in Tab 2.9. Every theoretically determined h lies within the experimentally determined margin of error. This indicates a successful demonstration of Lloyd's Mirror.

n	$h_{theory} \text{ (cm)}$	$h_{experimental} \text{ (cm)}$
1	9.68246	8.75 ± 0.75
2	13.8564	13.55 ± 0.75
3	17.1683	16.85 ± 0.75
4	20.0499	19.75 ± 0.75
5	22.6661	23.25 ± 0.75

Table 2.9: Experimental data of the Lloyd's mirror experiment. h_{theory} represents the theoretically determined heights of the ionosphere from the centre of the receiver horn which would induce a minimum intensity of microwave radiation. $h_{experimental}$ is the experimentally determined heights at which the ionosphere induces minimum transmission. Every theoretically determined h lies within the experimentally determined margin of error. This indicates a successful demonstration of Lloyd's Mirror.

The setup was not perfect as the metal sheet could not be reliably fixed face down. Due to its own weight, the free end of the mirror was often 'slumped' at a slight angle

to the table top. A suitable uncertainty was chosen for each measurement based on the variation of height at different points of the mirror when slumped.

2.7 Microwave Interferometry

This additional section explores interferometry techniques using microwaves.

An interferometer is a device that uses variations in the phase of a signal as it travels along distinct paths of adjustable length [9]. Optical Interferometers are used for wave-length and atmosphere refractive index measurements [17], gas flow measurements in wind tunnels [18] and recently they have been particularly important for Astrophysics and Astronomy [19]. An astronomical interferometer combines separate telescopes, mirror segments, or radio telescope antennas through interferometry to achieve higher-resolution imaging of celestial objects.

2.7.1 Michelson-Morley Interferometer

The Michelson-Morley experiment was first conducted in 1887 and sought to address the nature of the medium through which light waves propagate [20]. Here we demonstrate the setup's characteristics using microwaves apparatus.

Setup/Procedure

The experiment was setup as shown in Fig 2.13. First, we varied path length (ΔD_{path}) and noted interferometer output. We expect peak interferences for half-wavelength differences. By introducing a dielectric medium to one grid and measuring the distance a reflector must be moved to restore initial intensity, Δd , the refractive index of that material can be determined using

$$n = 1 + \frac{\Delta d}{t} \quad (2.7)$$

where t is the thickness of the material [21].

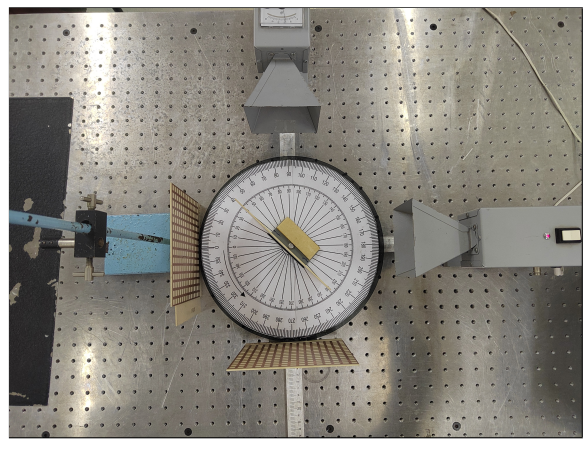
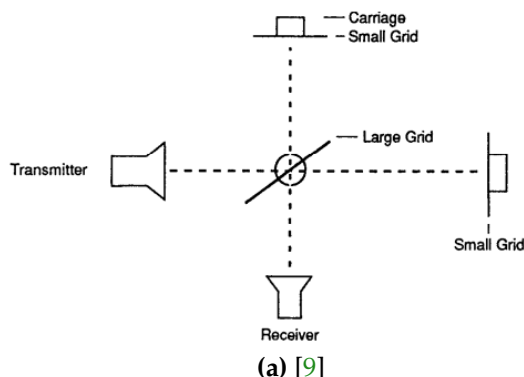


Figure 2.13: Experimental Setup of Michelson-Morley interferometer using 3cm microwave apparatus and accessories. Path length difference was varied by adjusting the position of the bottom grid in (b).

Results/Discussion

Resulting interference of microwaves due to a path length difference in the Michelson-Morley interferometer is demonstrated in Fig 2.14.

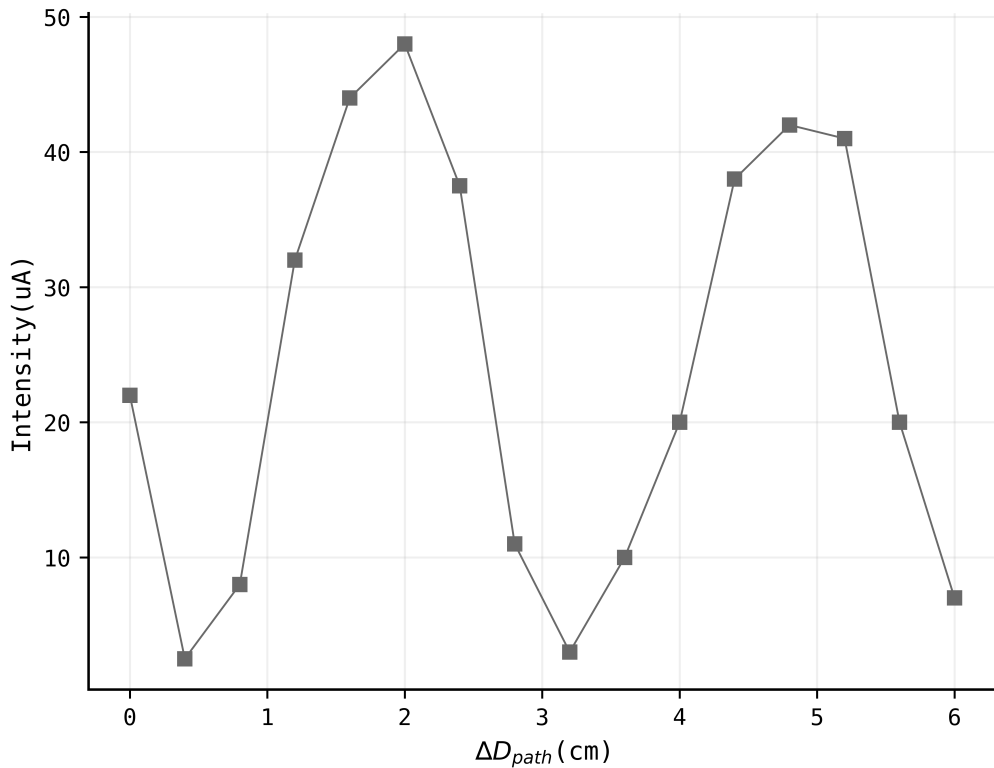


Figure 2.14: Experimental data of Michelson-Morley interferometer. Interference of microwaves due to a path length difference is demonstrated.

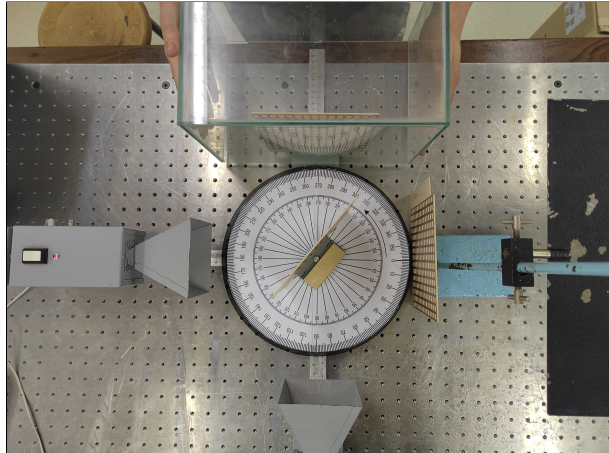


Figure 2.15: Fish tank inserted as dielectric medium. The fish tank was 4.5mm thick.

An old fish tank was found in the lab. It was decided to use this as our dielectric medium to take the refractive index measurement. The fish tank is imaged in Fig 2.15. The resulting change required to return to a minimum intensity was $\Delta d = (0.3 \pm 0.1)cm$. As such

$$n = 1 + \frac{0.3 \pm 0.1}{0.45} = 1.666 \pm 0.222$$

This result is within the margin of error for our previously determined n_{Glass} in Tab 2.7.

2.7.2 Fabry-Perot Interferometer

A Fabry-Perot interferometer is an optical device that employs multiple reflections between two parallel, partially reflecting mirrors to create interference patterns. It typi-

cally has practical applications in fibre optic sensing [22] and the underlying physics ("Fabry Perot Modes") appear throughout photonics.

Setup/Procedure

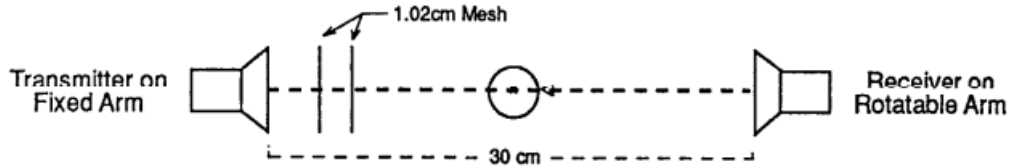


Figure 2.16: [9] Experimental setup of a Fabry-Perot interferometer using microwave apparatus and accessories.

The experiment was setup as shown in Fig 2.16. The distance between reflecting grids (labelled 'mesh' in Fig 2.16) was altered and the intensity was noted for various positions. We expect the observed interference with respect to ΔD_{grids} to be an Airy function [23].

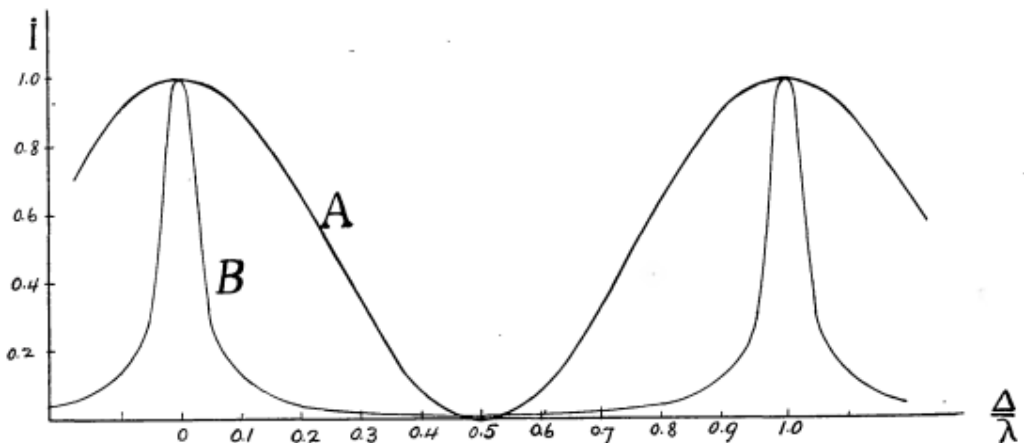


Figure 2.17: [23] FIG I from "On the Application of Interference Phenomena to the Solution of Various Problems of Spectroscopy and Metrology", where Fabry and Perot showed that curve B represents the law of variation of Intensity as a function of A or change in path length. Mathematically, it is an Airy function.

Results/Discussion

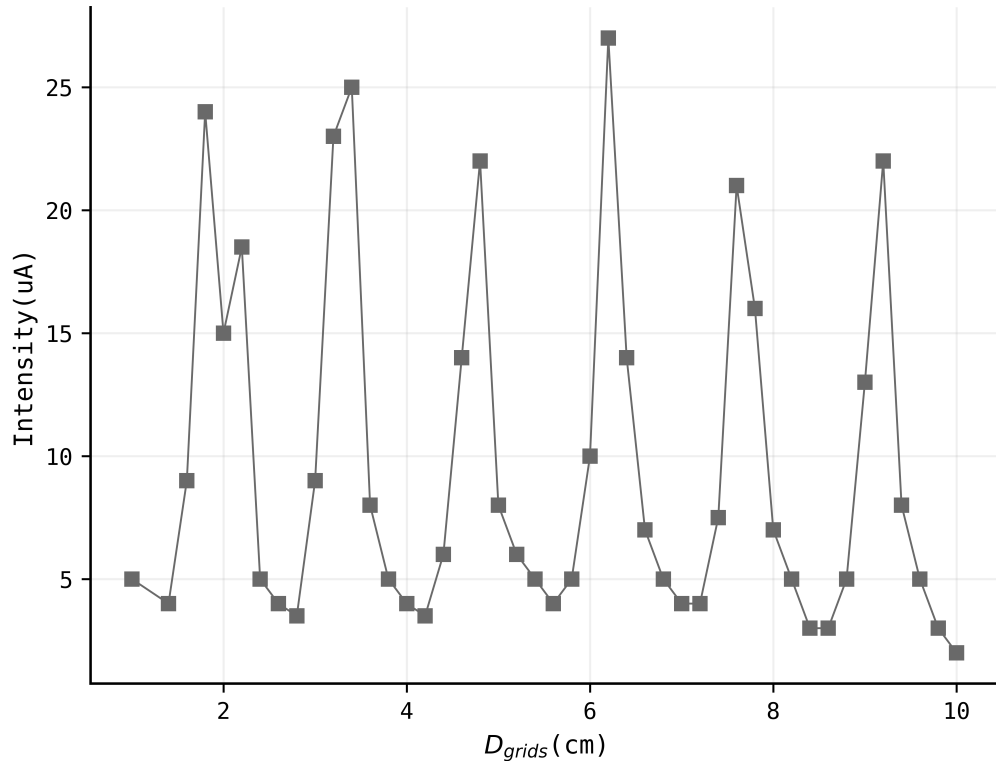


Figure 2.18: Resulting intensity-path length relationship is shown. It evidently holds the likeness of the function we expect to observe, the characteristic peaks of the airy function discussed are evident. The maxima locations do not align exactly with the expected locations according to [23], where the path length difference is approximately equal to the microwave wavelength.

Resulting intensity-path length relationship is shown in Fig 2.18. It evidently holds the likeness of the function we expect to observe, the characteristic peaks of the airy function are evident. The maxima locations do not align exactly with expected locations according to [23], where the path length difference is approximately equal to integer multiples of microwave wavelength. This may be due to measurement error during reading.

2.7.3 Thin Film Reflections

"Thin dielectric films exhibit frequency-sensitive interference effects due to the reflections at the front and back surfaces of the films."^[9] This experiment simulates this effect using a set of reflective grid mesh and microwaves.

Setup/Procedure

The experiment was setup as shown in Fig 2.19. The distance between mesh was altered iteratively and resulting intensity noted for each change. The interference with respect to mesh distance, D_{grids} , due to the reflections at the front and back surfaces of the films was then plotted.

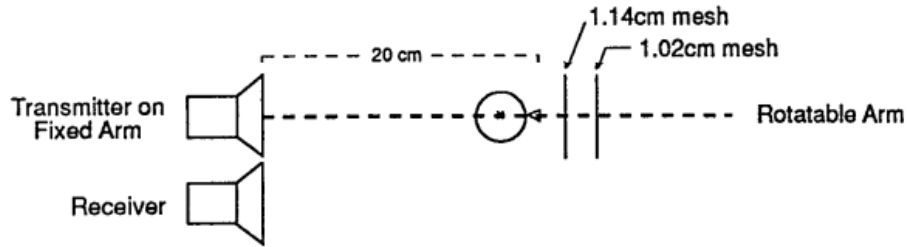


Figure 2.19: Thin film setup using microwave apparatus and accessories. The distance between mesh, D_{grids} , was altered iteratively and resulting intensity noted for each change.

Results/Discussion

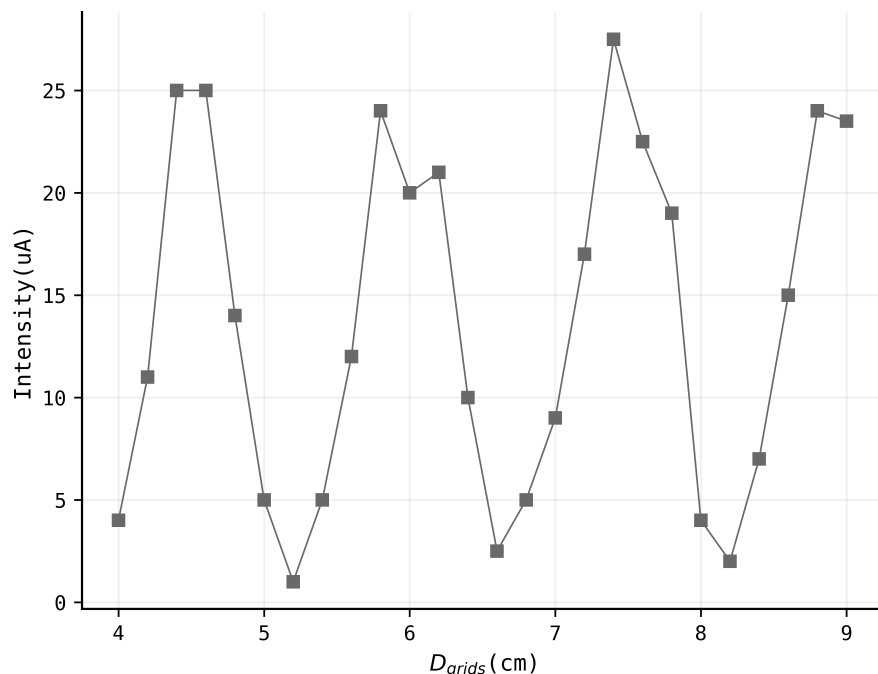


Figure 2.20: Thin film demonstration using microwaves. Signal level variations are affected by film thickness analogous to previous discussion. The distance between mesh, D_{grids} , was altered iteratively and resulting intensity noted for each change.

Fig 2.20 shows the results obtained using the outlined procedure. Signal level variations are affected by simulated film thickness analogous to previous discussion.

Further Discussion

Experiments/demonstrations were generally successful even though the apparatus had high potential for systematic error. The success is likely down to the waves themselves; a 3cm wavelength left room for human error.

However, this could also be due to the effort made to reduce systematic error by increasing the scale of measurements. At various points in the report procedure mod-

ifications were made to [9]. The setup was at times far from ideal. For example, in Fig 2.10 there is a distinct lack of symmetry in the results and it was very difficult to obtain these specific results. A close inspection of the apparatus placed horn-to-horn showed that they were misaligned (See Fig 3.21), perhaps a potential source of the difficulty considering the precision required to make a single-slit measurement at other wavelengths.



Figure 3.21: Difficulty in single slit measurements may have been due to misalignment of flared horns causing inaccuracies in measurement. The results in Fig 2.10 were not symmetrical.

It was disappointing that we could not show the relationship mentioned in [15] for the influence of humidity on microwave propagation. It could be done using a number of purpose built rectangular containers of variable thickness filled with various dielectrics. It is also disappointing that we had no access to salt to show that salt water overcomes the permittivity of pure water via ionic currents.

Conclusion

Various wave properties of microwaves are investigated. Polarisation effects are shown to hold at microwaves frequency and the law of reflection was successfully verified. The wavelength of transmitted microwaves were determined using standing waves and the speed of light calculated to high degree of accuracy. The phase wavelength was found for various setups using oblique standing waves and it appeared to not be a fixed quantity but depended on the perpendicular distance of the reflecting surface from the utilised apparatus. A similar demonstration is shown later in the report (Lloyd's mirror) which shows that these reflector distances can be accurately predicted for minimum intensity. Demonstrations of single and double slit diffraction patterns using microwaves gave comparable results to those of well-renowned historical studies. The refractive index of glass and paraffin wax are determined for microwaves and their significance are discussed in depth. The influence of humidity on microwaves is demonstrated but with little conclusion and rigour due to setup constraints. Interferometry techniques are investigated using microwaves as an additional activity.

Though lengthy, this report hopefully serves as a comprehensive and valid demonstration of the wave-properties of microwaves.

Bibliography

- [1] M. Vollmer, *Physics of the microwave oven*, **IOP Physics Education** **39**
- [2] Ziad F. Issa, John M. Miller, Douglas P. Zipes, *7 - Ablation Energy Sources, Clinical Arrhythmology and Electrophysiology (Third Edition)*,
- [3] C. Oliver Kappe, "Microwave dielectric heating in synthetic organic chemistry," **Organic Chemistry Society**, DOI: 10.1039/b803001b
- [4] J. C. Webber and M. W. Pospieszalski, "Microwave instrumentation for radio astronomy," **IEEE Transactions on Microwave Theory and Techniques**, vol. 50, no. 3, pp. 986-995, March 2002, doi: 10.1109/22.989982 **Elsevier**, 2019, Pages 206-237
- [5] R. Belén Barreiro, "The cosmic microwave background: State of the art," **New Astronomy Reviews**, Volume 44, Issue 3, 2000
- [6] Chr. Huygens "Treatise on Light: In Which Are Explained the Causes of That Which Occurs in Reflection & Refraction", **Macmillan**, 1912.
- [7] Q. Luo, Z. Wang and J. Han "A Padé approximant approach to two kinds of transcendental equations with applications in physics", *Eur. J. Phys.* **36** (2015) 035030 (14pp) [FIGURE 1]
- [8] M. Gondran, A. Gondran, "Measurement in the de Broglie-Bohm Interpretation: Double-Slit, Stern-Gerlach, and EPR-B", *Physics Research International*, vol. 2014, Article ID 605908, 16 pages, 2014. [FIGURE 4]
- [9] Three Centimeter Microwave Apparatus Operating Instructions, **Central Scientific Company**
- [10] "SI Brochure: The International System of Units (SI) (9 ed.)," BIPM, 2019, p. 128, retrieved 2020-01-12 **Bureau International des Poids et Mesures**
- [11] "Optical Glass", Data Sheet, **SCHOTT** - access via www.refractiveindex.info
- [12] V. V. Bassarab et al 2023 *J. Opt.* **25** 065401
- [13] S. Singh 2002 *Phys. Scr.* **65** 167
- [14] R. B. Breite, "Reflection, transmission and refraction of microwaves", Student's Sheet, **PHYWE**

- [15] M. Pieraccini, A. Bicci, D. Mecatti, G. Macaluso and C. Atzeni, "Propagation of Large Bandwidth Microwave Signals in Water," in **IEEE Transactions on Antennas and Propagation**, vol. 57, no. 11, pp. 3612-3618, Nov. 2009, doi: 10.1109/TAP.2009.2025674.
- [16] Lloyd, Humphrey. "On a New Case of Interference of the Rays of Light." The Transactions of the Royal Irish Academy, vol. 17, 1831, pp. 171–77. JSTOR
- [17] H. Matsumoto, Y. Zhu, S. Iwasaki, T. O'ishi, "Measurement of the changes in air refractive index and distance by means of a two-color interferometer," Appl. Opt. 31, 4522-4526 (1992)
- [18] M. R. Fulghum "Turbulence measurements in high-speed wind tunnels using focusing laser differential interferometry," The Pennsylvania State University ProQuest Dissertations Publishing, 2014. 3690119.
- [19] O. von dcr Lühe, "An Introduction to Interferometry with the ESO Very Large Telescope", European Southern Observatory
- [20] R. S. Shankland, "Michelson-Morley Experiment" Am. J. Phys. 1 January 1964; 32 (1): 16–35
- [21] EXPERIMENT 5 Microwave Michelson Interferometer, Lab brief, University of Louisville
- [22] L. C. Gunderson, "Fiber optic sensor applications using Fabry-Perot interferometry", Proc. SPIE 1267, Fiber Optic Sensors IV, (1 August 1990)
- [23] A. Perot, C. Fabry, "On the Application of Interference Phenomena to the Solution of Various Problems of Spectroscopy and Metrology", Astrophysical Journal, vol. 9, p.87